Bioorganic & Medicinal Chemistry Letters 29 (2019) 383–388

Contents lists available at ScienceDirect

Bioorganic & Medicinal Chemistry Letters

journal homepage: www.elsevier.com/locate/bmcl

Synthesis, biological evaluation and 3D-QSAR studies of 1,2,4-triazole-5-substituted carboxylic acid bioisosteres as uric acid transporter 1 (URAT1) inhibitors for the treatment of hyperuricemia associated with gout

Jing-wei Wu[a], Ling Yin[b], Yu-qiang Liu[c], Huan Zhang[d], Ya-fei Xie[c], Run-ling Wang[a,*], Gui-long Zhao[c,*]

[a] Tianjin Key Laboratory on Technologies Enabling Development of Clinical Therapeutics and Diagnostics (Theranostics), School of Pharmacy, Tianjin Medical University, Tianjin 300070, PR China
[b] Department of Chemistry and Chemical Engineering, Jining University, Qufu 273155, PR China
[c] Tianjin Key Laboratory of Molecular Design and Drug Discovery, Tianjin Institute of Pharmaceutical Research, Tianjin 300193, PR China
[d] General Hospital, Tianjin Medical University, Tianjin 300052, PR China

ARTICLE INFO

(Dedicated to Professor Jian-wu Wang on the occasion of his 65th birthday)

Keywords:
Synthesis
Biological evaluation
3D-QSAR
Bioisosteres
Gout

ABSTRACT

As a part of our ongoing research to develop novel URAT1 inhibitors, 19 compounds (**1a-1s**) based on carboxylic acid bioisosteres were synthesized and tested for in vitro URAT1 inhibitor activity (IC_{50}). The structure-activity relationship (SAR) exploration led to the discovery of a highly potent novel URAT1 inhibitor **1g**, which was 225-fold more potent than the parent lesinurad in vitro (IC_{50} = 0.032 μM for **1g** against human URAT1 vs 7.20 μM for lesinurad). Besides, 3D-QSAR pharmacophore models were established based on the activity of the compounds (**1a-1s**) by Accelrys Discovery Studio 2.5/HypoGen. The best hypothesis, Hypo 1, was validated by three methods (cost analysis, Fisher's randomization and leave-one-out). Although compound **1g** is among the most potent URAT1 inhibitors currently under development in clinical trials, the Hypo1 appears to be favorable for future lead optimization.

Gout is a prototypical inflammatory disease which has been proved difficult to treat. The past decades have witnessed an increase in prevalence and incidence in both developing and developed countries.[1] Clinically, gout is characterized by acute inflammatory arthritis, tophi, articular erosions and uric acid renal stones.[2,3] Hyperuricemia is associated with an increased risk of gout due to an abnormally elevated concentration of serum uric acid above its saturation point in physiological fluid (sUA levels > 6.8 mg/dL, i.e. 404 μmol/L).[4] In view of severe pain, kidney stone and possible bone erosion, patients with gout and hyperuricemia are in urgent need of effective strategy to reduce sUA levels.[5]

Urate is the final metabolic product of purines both exogenous and endogenous owing to lack of uricase. Uricase is an enzyme that oxidizes insoluble uric acid to soluble allantoin which can be excreted via kidney.[6,7] Most of the urate filtered by the kidney is reabsorbed, this process is mediated by uric acid transporters, which fall into two categories: urate reabsorption transporters and urate excretion transporters. The major transporter involved in this process is urate transporter 1 (URAT1), a protein possessing 555 amino acid residues and first identified in Xenopus oocytes, which plays a key role in maintaining serum uric acid level.[8] Some URAT1 inhibitors, such as probenecid and benzbromarone (Figure 1), promote the excretion of uric acid by inhibiting URAT1 to block the reabsorption of uric acid. However, probenecid is associated with low efficacy, short harf-life and side effects of gastrointestinal irritation and rash, and should take caution in elderly patients and those with CrCl (creatinine clearance) < 50 mL/min.[9] Benzbromarone is more potent than probenecid, however it should be avoided in patients with eGFR (estimation of glomerular filtration rate) < 30 mL/min because of hepatotoxicity, which lead to its withdrawal from the Europe in 2003.[10] Lesinurad (Figure 1), a selective URAT1 inhibitor, was approved for use in combination with a xanthine oxidase inhibitor (XOI) for the treatment of hyperuricemia associated with gout in the United States in December 2015 and in the European Union in 2016.[9] However, Lesinurad suffers from low efficacy and narrow therapeutic window.[11]

In the effort of discovering potent inhibitors based on the structure of lesinurad in our laboratories, earlier studies successfully found a highly potent inhibitor **1**, whose IC_{50} values are even lower by almost

* Corresponding authors.
E-mail addresses: wangrunling@tmu.edu.cn (R.-l. Wang), zhao_guilong@126.com (G.-l. Zhao).

https://doi.org/10.1016/j.bmcl.2018.12.036
Received 13 November 2018; Received in revised form 14 December 2018; Accepted 16 December 2018
Available online 17 December 2018
0960-894X/

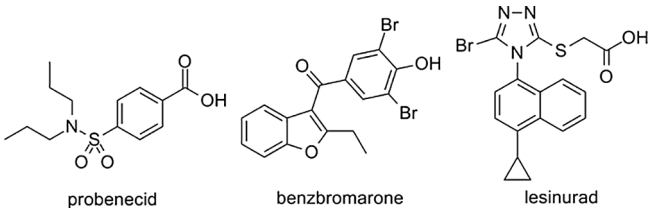

Figure 1. Structures of approved URAT1 inhibitors.

two orders of magnitude than lesinurad (Figure 2).[12] Intensive study of structure–activity relationship (SAR) of lesinurad has been performed in earlier studies.[12–14] except the carboxylic acid moiety in lesinurad. As a continuation of the earlier studies, in the present study we first designed and synthesized a series of compounds with a variety of carboxylic acid bioisosteres.[15,16] based on compound **1** (**1a-1g** in Figure 2). Fortunately, we discovered a more potent URAT1 inhibitor **1g** compared with **1**, which bears a N-(pyridin-3-yl)sulfonamide moiety and was 225-fold more potent than lesinurad in *in vitro* URAT1 inhibitory assay (IC_{50} = 0.032 μM for **1g** against human URAT1 vs 7.20 μM for lesinurad) (Figure 2). Encouraged by this promising finding, we further designed and synthesized 12 derivatives (**1h-1s**) of compound **1g** to explore the substitution on the pyridine nucleus in the newly discovered N-(pyridin-3-yl)sulfonamide, but none of them were found to be more active than **1g**. As shown in Table 1, compound **1g** is among the most potent URAT1 inhibitors currently under development in clinical trials and a promising drug candidate for further development.

The synthetic route to desired products **1a-1e** was shown in Scheme 1. Regioselective S-alkylation of triazoline-3-thione (**2**) with $ICH_2CH_2CO_2Et$ in the presence of K_2CO_3 in DMF at room temperature smoothly afforded **3** according to known procedures.[24] The bromination at 5-position of the 1,2,4-triazole ring in **3** with *N*-bromosuccinimide (NBS) in MeCN at 30–40 °C afforded **4**.[12] Treatment of **4** with aqueous LiOH in MeOH at room temperature according to the known procedure[24] triggered the *retro*-Michael addition, yielding 5-bromotriazoline-3-thione **(5)** by cleavage of the propionate protecting group. Regioselective S-alkylations of **5** with 2,6-dibromo-4-(bromomethyl)

Table 1
Profiles for URAT1 inhibitors approved and under development in clinical trials.

Code name	Generic name	Originator company	Development status	IC_{50} (μM)
–	Probenecid	Merck	Approved	13.23[17]
–	Sulfinpyrazone	Novarits	Approved	32[18]
–	Benzbromarone	–	Approved	0.22[18]
RDEA594	Lesinurad	Ardea	Approved	7.3[11]
RDEA3170	Verinurad	Ardea	Phase II	0.024[19]
URC-102	–	JW	Phase II	0.057(K_i)[20]
MBX-102	Arhalofenate	Cyma Bay	Phase II	92[21]
–	Tranilast	Nuon	Phase II	24[22]
SHR4640	–	Hengrui	Phase II	0.0337[23]

phenol,[25] $ClCH_2SO_2NH_2$,[26] 5-chloromethyl-1H-tetrazole[27] or $BrCH_2SO_2ONa$[28] needs KI as catalyst to accelerate the reaction. Thus, treatment of thione **5** with the above four alkylating reagents in the presence of KI as catalyst and K_2CO_3 as base in DMF at elevated temperatures (80 °C for **1a**, 50 °C for **6b**, 80 °C for **1d** and 130 °C for **6e**) produced **1a**, **6b**, **1d.**[29] or **6e**, respectively. Compounds **6b** and **6e** were converted to corresponding sodium salts **1b** and **1e**, respectively, to improve the solubility in water that was desired in *in vitro* URAT1 inhibitory assay. Regioselective S-alkylations of **5** with $BrCH_2CO_2CH_3$ in the presence of K_2CO_3 in DMF at room temperature gave ester **6c**.[12] **6c** was converted to target hydroxamic **1c** by treatment with hydroxylamine hydrochloride in the presence of KOH in MeOH at room temperature.

The synthetic route to desired products **1f-1s** was shown in Scheme 2. Sulfonylation of aniline (**7f**) with 1 eq of $ClCH_2SO_2Cl$ (**6**) in the presence of pyridine in dried CH_2Cl_2 at 0 °C to room temperature smoothly produced **9f**.[30] however, under the same reaction condition, aminopyridines **7g-7s** gave predominantly *N,N*-bis-sulfonylated derivatives **8g-8s** in low yields. So we adopted another known two-step procedure involving bissulfonation followed by monodesulfonation.[31] Thus, treatment of aminopyridines **7g-7s** with 2 eq of $ClCH_2SO_2Cl$ (**6**) in the presence of triethylamine in dried CH_2Cl_2 at 0 °C to room

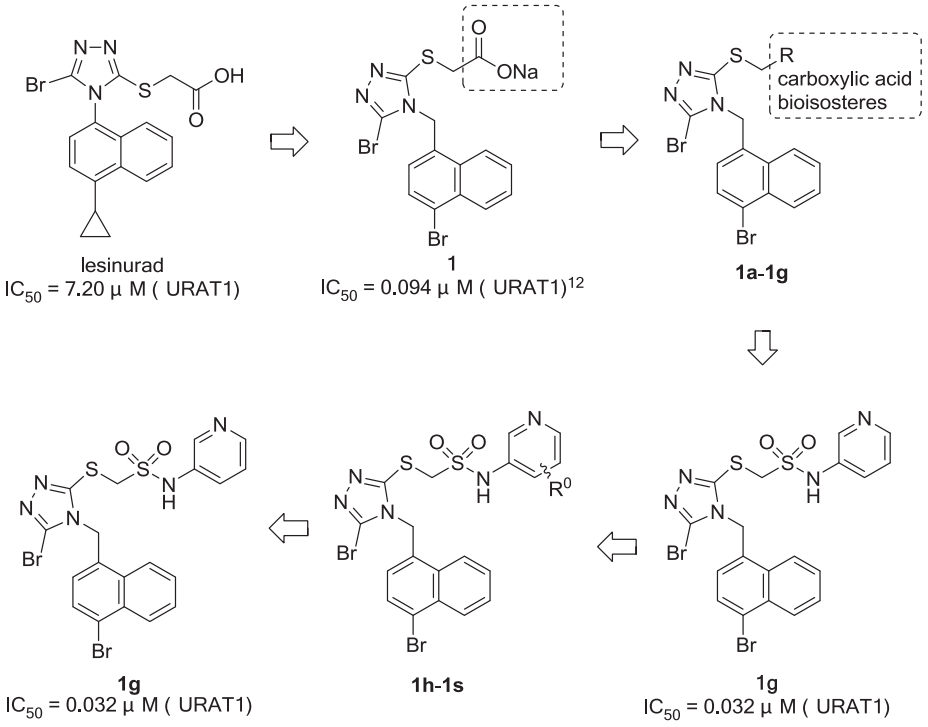

Figure 2. Design of URAT1 inhibitors in present study.

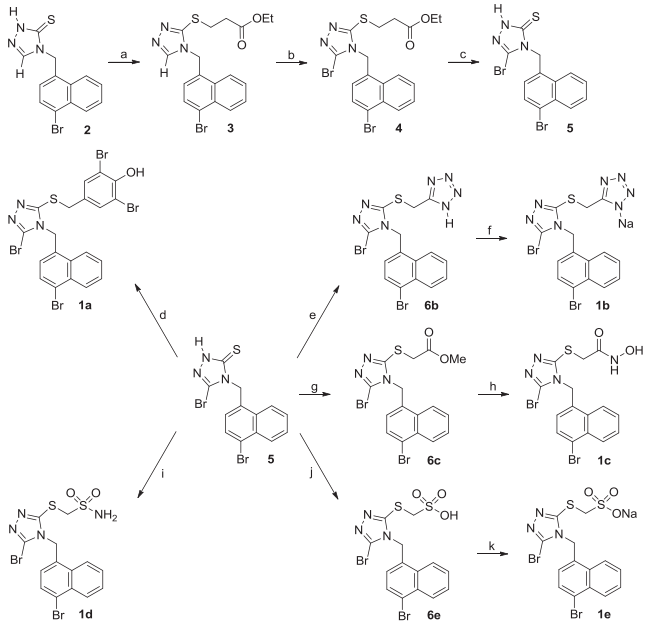

Reagents and conditions: a. $ICH_2CH_2CO_2Et$, K_2CO_3, DMF, 0℃-r.t.; b. NBS, MeCN, 30-40°C; c. aq LiOH, MeOH, r.t.; d. 2,6-dibromo-4-(bromomethyl)phenol, KI, K_2CO_3, DMF, 80°C, N_2; e. 5-chloromethyl-1H-tetrazole, KI, K_2CO_3, DMF, 50°C, N_2; f. aq NaOH, MeOH, r.t.; g. $BrCH_2CO_2CH_3$, K_2CO_3, DMF, r.t., N_2; h. $NH_2OH{\cdot}HCl$, KOH, MeOH, r.t.; i. $ClCH_2SO_2NH_2$, KI, K_2CO_3, DMF, 80°C, N_2; j. (1) $BrCH_2SO_2ONa$, KI, K_2CO_3, DMF, 130°C, N_2; (2) aq HCl. k. aq NaOH, MeOH, r.t..

Scheme 1. Synthetic approach to desired products **1a-1e,** Reagents and conditions: a. $ICH_2CH_2CO_2Et$, K_2CO_3, DMF, 0 ˚C -r.t.; b. NBS, MeCN, 30–40 ˚C; c. aq LiOH, MeOH, r.t.; d. 2,6-dibromo-4-(bromomethyl)phenol, KI, K_2CO_3, DMF, 80 ˚C, N_2; e. 5-chloromethyl-1H-tetrazole, KI, K_2CO_3, DMF, 50 ˚C, N_2; f. aq NaOH, MeOH, r.t.; g. $BrCH_2CO_2CH_3$, K_2CO_3, DMF, r.t., N_2; h. $NH_2OH{\cdot}HCl$, KOH, MeOH, r.t.; i. $ClCH_2SO_2NH_2$, KI, K_2CO_3, DMF, 80 ˚C, N_2; j. (1) $BrCH_2SO_2ONa$, KI, K_2CO_3, DMF, 130 ˚C, N_2; (2) aq HCl. k. aq NaOH, MeOH, r.t.

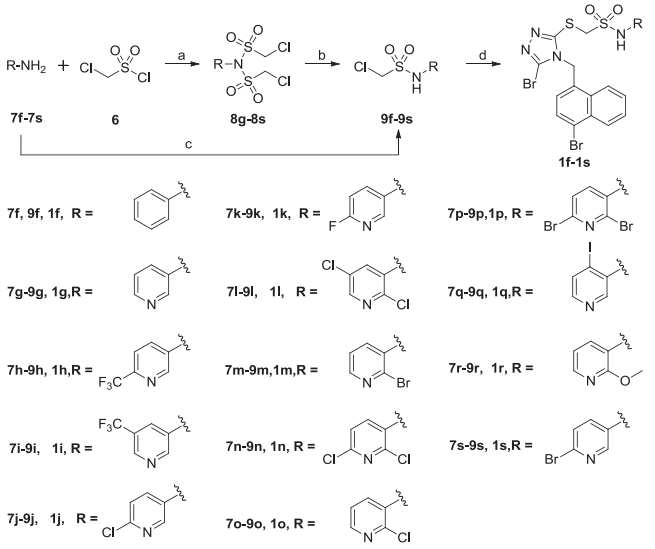

Reagents and conditions: a. Et_3N, dried CH_2Cl_2, 0°C -r.t.; b. (1) 10% NaOH, 0°C -r.t.; (2) aq HCl, 0°C -r.t.; c. **7**f: pyridine, dried CH_2Cl_2, 0°C -r.t.; d. **5**, KI, K_2CO_3, DMF, 80°C (**1f**) or 130°C (**1g-1s**), N_2.

Scheme 2. Synthetic approach to desired products **1f-1 s.** Reagents and conditions: a. Et_3N, dried CH_2Cl_2, 0 ˚C -r.t.; b. (1) 10% NaOH, 0 ˚C -r.t.; (2) aq HCl, 0 ˚C -r.t.; c. **7**f: pyridine, dried CH_2Cl_2, 0 ˚C -r.t.; d. **5**, KI, K_2CO_3, DMF, 80 ˚C (**1f**) or 130 ˚C (**1g-1s**), N_2.

Table 2
Results for in vitro assays of the synthesized compounds **1a-1s** and parent compounds (lesinurad and **1**) against human URAT1.

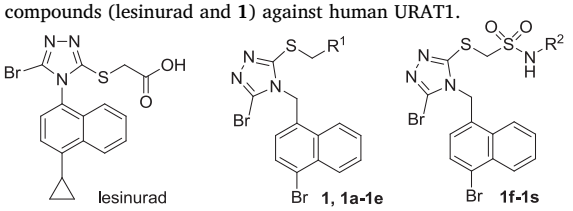

Compound	R^1	R^2	IC_{50} (μM)
lesinurad	–	–	7.20[a]
1	CO_2H	–	0.094 ± 0.012
1a	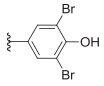	–	119 ± 23
1b		–	3.24 ± 0.65
1c	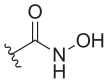	–	0.64 ± 0.11
1d	$-SO_2NH_2$	–	365 ± 55
1e	$-SO_2ONa$	–	14.38 ± 2.02
1f	–		15.78 ± 1.97
1g	–		0.032 ± 0.0051
1h	–	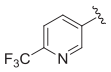	10.21 ± 1.68
1i	–	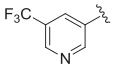	6.38 ± 1.68
1j	–	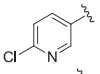	1.94 ± 0.40
1k	–		1.55 ± 0.28
1l	–	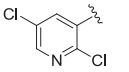	2.79 ± 0.50
1m	–	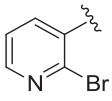	0.28 ± 0.042
1n	–	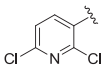	1.66 ± 0.22
1o	–	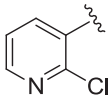	5.10 ± 0.76
1p	–	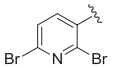	5.41 ± 0.77
1q	–		10.57 ± 2.4
1r	–	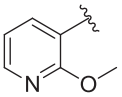	4.05 ± 0.69
1s	–	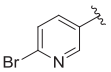	2.2 ± 0.23

[a] Reported value for lesinurad: IC_{50} = 7.3 μM against human URAT1.[11]

temperature produced corresponding *N*,*N*-bis-sulfonylated intermediates **8g-8s**, which were in turn monodesulfonylated to furnish the desired *N*-pyridinylmethanesulfonamides (**9g-9s**) by treatment with 10% aqueous NaOH at 0 °C to room temperature. Finally, regioselective S-alkylation of **5** with **9g-9s** in the presence of KI as catalyst and K_2CO_3 as base in DMF at 130 °C produced the final desired products **1f-1s**.

The results of in vitro inhibitory assay of 19 synthesized compounds (**1a-1s**) as well as lesinurad as positive control against human URAT1 are summarized in Table 2. As shown in Figure 2, to find an optimal nucleus for the carboxylic acid bioisostere, the first round of SAR exploration in this study started with the carboxylic acid bioisosteres of compound **1**. Thus, we replaced the carboxylic acid moiety with those in **1a-1g** (Table 2) because they are considered to be typical carboxylic acid bioisosteres.[15,16] It is very clear that among all the carboxylic acid bioisosteres explored (**1a-1g**), only the N-(pyridine-3-yl)sulfonamide nucleus is more potent than the parent carboxylic acid as indicated by the 2.9-fold improvement in IC_{50} value of **1g** vs **1** (IC_{50} = 0.032 μM for **1g** vs 0.094 μM for **1**).

In the second round of SAR exploration, we in turn focused on the fine tuning of the substituents around N-(pyridine-3-yl)sulfonamide nucleus discovered in the first round. Thus, compounds **1h-1s** were designed. Unfortunately, none of these compounds displayed more potent URAT1 inhibitory activity compared with **1g**, indicating that the N-(pyridine-3-yl)sulfonamide can not tolerate any substitution.

In summary, two round of SAR exploration led to the discovery of a highly active novel inhibitor **1g**, which was 225- and 3-fold more potent than the parent compounds lesinurad and **1** (IC_{50} = 0.032 μM for **1g** vs 7.20 μM for lesinurad and 0.094 μM for **1**), respectively. However, the IC_{50} values for these 1,2,4-triazole-5-substituted carboxylic acid bioisosteres (**1a-1s**) ranged from 0.032 μM to 365 μM, which span four orders of magnitude. With the aim to obtain additional information of the relationship between structure and activity and to discover more active URAT1 inhibitors, 3D-QSAR studies were carried out.

Based on the biological activity values (IC_{50}) of the investigated compounds (**1a-1s**), 3D-QSAR pharmacophore models were established within *Accelrys Discovery Studio 2.5* software using *HypoGen*[32–34] module. As the training set compounds, **1a-1s** were in accord with the selection rule in *HypoGen*: at least 16 diverse inhibitors (a total of 19 compounds including **1a-1s**) to ensure statistical significance and the biological activities span at least four orders of magnitude (0.032 μM ~ 365 μM). All compounds in training set were classified into four activity scales: highly active ($IC_{50} \leq$ 200 nM, + + +), active (200 nM < $IC_{50} \leq$ 2 μM, + +), moderately active (2 μM < $IC_{50} \leq$ 20 μM, +), inactive (IC_{50} > 20 μM, -). This classification is helpful to generate and evaluate the pharmacophore model with abroad range of activities quickly.[35] Structures of the training set (**1a-1s**) were imported into *Discovery Studio* and energy minimized to the closest local minimum using the generalized CHARMM force field by *Minimized Ligands* algorithm. Meanwhile, conformational ensembles of the local minimized structure with a maximum limit of 255 conformers per molecule were generated within *Conformation Generation* module by best methods and using an energy threshold of 20 kcal/mol.[36] A list of pharmacophore feature types for the training set, such as hydrogen bond acceptors (HBA), hydrogen bond doners (HBD), hydrophobic (HY) and ring aromatic (RA), were represented in *Edit and Cluster Features* module. The minimum numbers of each feature type were set to 1 and the maximum numbers of them were set to 3. With the help of *3D QSAR Pharmacophore Generation* tool, the pharmacophore models were established by three major steps: the constructive phase (generation of the common pharmacophores among the active training molecules), the subtractive phase (elimination of the pharmacophores that are common to most of the inactive molecules) and the optimization phase (attempt to improve the score by applies small perturbation to the pharmacophores created in constructive and subtractive phases).[37]

As shown in Table 3, HypoGen provided the top 10 scoring hypotheses, Hypo1 was the best one of them because it had the highest correlation coefficient (R^2), lowest total cost (97.988), highest cost difference (72.207), and a low root mean squared deviation (RMSD) values. The correlation coefficient value (R^2) and RMSD values for Hypo 1 were 0.9477 and 1.6004, respectively.

The predictive ability of Hypo 1 on the training set compounds was shown in Table 4. In accordance with the Hypo1 activity values, 17 out of 19 compounds in the training set were predicted within their experimental activity scale except **1b** and **1f.** The error value is the ratio between the estimated and experimental activities. An absolute value of error below 10 indicates that the estimated activity was below one order of magnitude. None of the 19 training-set compounds had an absolute value of error above 4. Fit value can provide information in understanding the chemical meaning of the pharmacophore hypothesis by overlaping the molecule chemical features in the pharmacophore. The fit value of the most active compound (**1g**) of the training set was 10.45 while the least active compound (**1d**) was 7.27. All these datas suggested that Hypo 1 was a reliable model with high predictive ability.

The pharmacophore mapping of the most active (**1g**) compound, the parent compound (**1**) and the least active compound (**1d**) were shown in Figure 3A, B and C, respectively. Obviously, compound **1g** mapped well on three hypothetical features, while compound **1d** did not map on to two of the hypothetical features, particularly HBA and HBD, signifying the importance of these features. Moreover, the parent compound **1** mapped on two hypothetical features (i.e. HBD and HY features). As shown in Figure 3A and B, both **1** and **1g** mapped the feature of hydrogen bond doners (magenta), which provided by carboxylic acid bioisostere. By comparison with compound **1**, **1g** had proved to be one of the best carboxylic acid bioisosteres. Therefore, Hypo1 is a reliable model that accurately estimates the experimental activity of the training-set compounds.

Finally, the best pharmacophore model, Hypo1, was further validated by cost analysis, Fischer randomization and leave-one-out methods.

The quality of a pharmacophore model is evaluated primarily by using two theoretical cost calculations that are represented in bit units. One is the “null cost” representing the highest cost of a pharmacophore model with no features; this value estimates every activity as the averaged activity data from the training-set compounds. The second cost is the “fixed cost,” which represents the simplest model that fits all the data perfectly. The total cost should always be far from the null cost and near the fixed cost when developing a meaningful model. The null cost of the ten established pharmacophore models was 170.195 bits, and the fixed cost was 62.375 bits. The analysis of ten generated pharmacophore models indicated that the total cost value for Hypo 1 is the closest to the fixed cost value than other models. The cost difference between the null cost and total cost value of Hypo 1 is 72.207 bits (Table 3). So Hypo 1 exhibited strong predictive capacity (If the difference is > 60 bits, the model has brilliant ability to fit all the data; when the difference is 40–60 bits, there is a 75–90% chance that it represents the data well; if the difference is under 40, it does not fit all the data).[38,39] The configuration cost was 16.1228, which is less than the maximum threshold of 17.[40]. Cost analysis confirms that the hypotheses had rational correlations.

Secondly, to verify whether the pharmacophore model had a strong correlation between the structure of the training set compounds (**1a-1s**) and the biological activities, a Fischer randomization test was carried out.[41] The parameters of the randomized pharmacophore model were the same as those used to generate the original one. 19 different randomizations were generated to achieve a 95% confidence level that the best pharmacophore Hypo 1 was not generated by chance.[42] The total costs of Hypo 1 and 19 randomized pharmacophore models were shown in Figure 4. Apparently, none of these 19 new hypotheses had lower cost values than the true hypothesis. This test shows that the Hypo 1 was not generated by chance, and that there is a probability of at least a 95% that it shows a valid correlation between chemical structure and URAT1 inhibitory activity.[43]

Table 3
Statistical results of the 10 pharmacophore hypothesis generated by HypoGen.

Hypothesis	Total cost	Cost Difference[a]	RMSD	Correlation	Features[b]
Hypo 1	97.988	72.207	1.6004	0.9477	HBA + HBD + 2HY
Hypo 2	98.164	72.031	1.9002	0.9209	2HBA + HY + RA
Hypo 3	100.176	70.019	1.9150	0.9195	HBA + HY + RA
Hypo 4	103.614	67.019	2.2121	0.8932	HBA + 2RA
Hypo 5	104.376	65.819	2.6342	0.8410	HBA + HY + RA
Hypo 6	106.654	63.541	2.5832	0.8484	HBA + 2RA
Hypo 7	108.397	61.798	2.7706	0.8223	2HBA + HBD + HY
Hypo 8	109.814	60.381	2.7794	0.8211	2HBA + HY + RA
Hypo 9	110.160	60.035	2.7869	0.8200	2HBA + HY + RA
Hypo 10	110.422	59.773	2.6853	0.8354	HBA + 2RA

[a] Cost difference = null cost – total cost; Null cost = 170.195; fixed cost = 62.375; confguration cost = 16.1228.
[b] HBA, hydrogen bond acceptor; HBD, hydrogen bond donor; hydrophobic,HY; ring aromatic, RA.

Table 4
Experimental and estimated IC_{50} values of the training set compounds based on best pharmacophore Hypo 1.

Name	IC_{50}(μM)		Error[a]	Fit Value[b]	Activity Scale[c]	
	Estimate	Experimental			Estimate	Experimental
1g	0.07	0.032	2.2	10.45	+ + +	+ + +
1m	0.28	0.28	−1	9.86	+ +	+ +
1c	1.4	0.64	2.2	9.14	+ +	+ +
1k	1.7	1.6	1.1	9.06	+ +	+ +
1n	2	1.7	1.2	9	+ +	+ +
1j	2	1.9	1	9	+ +	+ +
1s	5.1	2.2	2.3	8.59	+	+
1l	6.1	2.8	2.2	8.51	+	+
1b	1.2	3.2	−2.6	9.21	+ +	+
1r	2.9	4	−1.4	8.84	+	+
1o	7.6	5.1	1.5	8.42	+	+
1p	8.6	5.4	1.6	8.36	+	+
1i	6.7	6.4	1.1	8.47	+	+
1h	5.5	10.2	−1.9	8.56	+	+
1q	6.2	10.6	−1.7	8.5	+	+
1e	4	14.4	−3.6	8.69	+	+
1f	23	15.8	1.4	7.94	–	+
1a	140	119	1.2	7.15	–	–
1d	110	365	−3.4	7.27	–	–

[a] Error: Positive value indicates that the estimate IC_{50} is higher than the experimental IC_{50}; negative value indicates that the estimate IC_{50} is lower than the experimental IC_{50}.
[b] Fit value indicates how well the features in the pharmacophore map the chemical features in the compound.
[c] Activity Scale: highly active ($IC_{50} \leq 200$ nM, + + +), active (200 nM $< IC_{50} \leq$ 2 μM, + +), moderately active (2 μM $< IC_{50} \leq$ 20 μM, +), inactive ($IC_{50} >$ 20 μM, -).

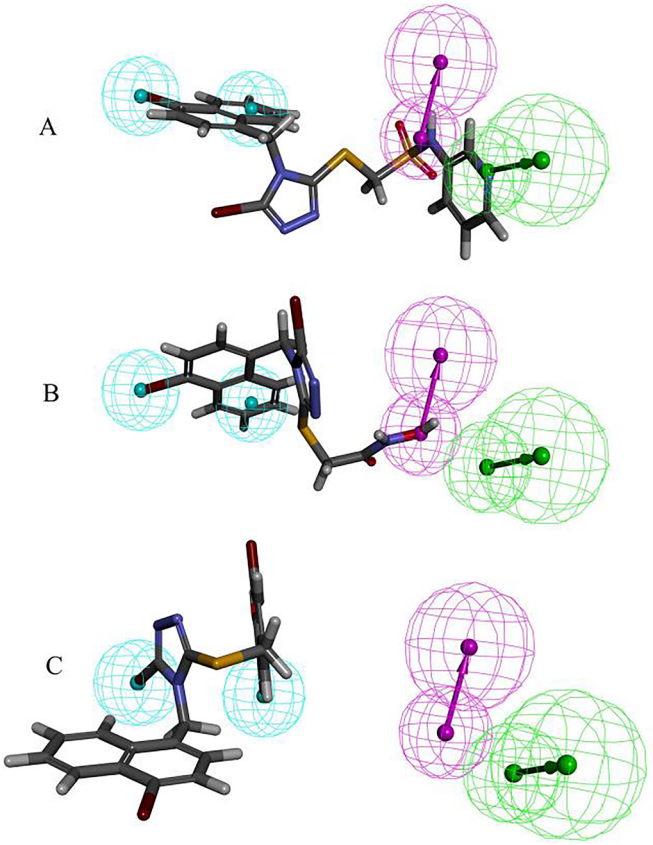

Figure 3. Alignment of hypotheses to training set compounds. (A) most active compound **1g** (IC_{50} = 0.032 μM), (B) parent compound **1** (IC_{50} = 0.094 μM) and (C) least active compound **1d** (IC_{50} = 365 μM). In the pharmacophore model - green represents HBA, magenta represents HBD and cyan represents HY features.

Thirdly, Hypo 1 was validated using a leave-one-out method, which used to verify if the correlation between the experimental and predicted activities was primarily dependent on one particular compound in the training set, or otherwise.[44] This was done by applying recursive iteration on the pharmacophore model by excluding one molecule in every iteration cycle.[45] 19 new training sets were derived and each of them contained 18 compounds. The 19 HypoGen calculations were carried out under conditions that were identical to the ones used in the generation of Hypo 1. The correlation coefficients of newly generated pharmacophore models were computed and no meaningful differences were found between Hypo1 and any of the pharmacophore models resulting from the leave-one-out method. This result enhances the confidence level of Hypo 1 did not depend solely on one particular molecule in the training set.

In conclusion, bioisosteric replacement of the carboxylic acid moiety in compound **1** resulted in the identification of a highly potent URAT1 inhibitor **1g**, which bears a N-(pyridin-3-yl)methanesulfonamide moiety and is 225-fold more potent than the parent lesinurad (IC_{50} = 0.032 μM for **1g** vs 7.20 μM for lesinurad). Compared to the potent URAT1 inhibitors discovered early, compound **1g** is the most potent URAT1 inhibitor discovered in our laboratories so far and also among the most potent ones currently under development in clinical trials. It is a very promising potential drug candidate for the treatment of hyperuricemia associated with gout. 3D-QSAR analysis was performed to rationalize the activity data for these 1,2,4-triazole-5-substituted carboxylic acid bioisosteres. Hypo 1, as the best pharmacophore model generated by Accelrys Discovery Studio 2.5/HypoGen, was proved to be a reliable model and favorable for future lead optimization.

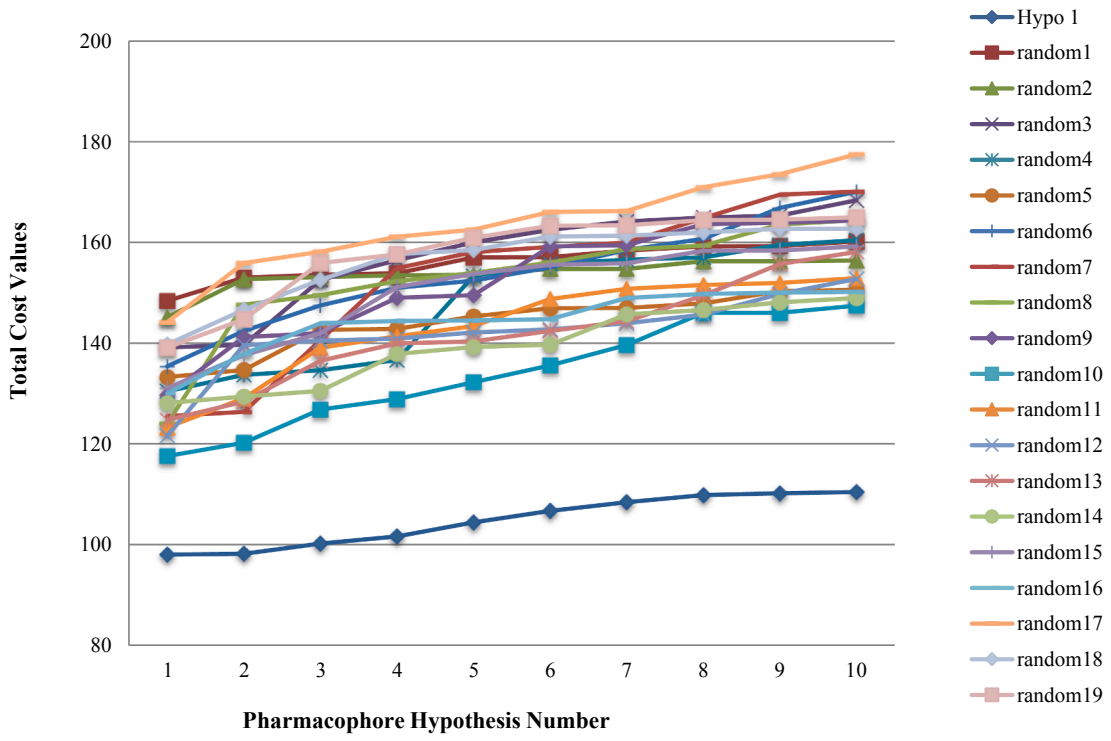

Figure 4. Fisher's randomization test results.

Acknowledgments

This study was supported by the National Natural Science Foundation of China (Grant No. 81273361), the Natural Science Foundation of Tianjin (Grant No.16JCZDJC32500), the International (Regional) Cooperation and Exchange Project of the National Natural Science Foundation of China (Grant No. 81611130090).

Appendix A. Supplementary data

Supplementary data to this article can be found online at https://doi.org/10.1016/j.bmcl.2018.12.036.

References

1. Song G, Wang R, Guo J, et al. *Sci Rep.* 2015;5:15793.
2. Richette P, Bardin T. *The Lancet.* 2010;375:318.
3. Zhang XW, Liu N, Chen S, et al. *Oncol Lett.* 2015;10:410.
4. Li X, Li X, Liao D, et al. *Curr Protein Pept Sci.* 2015;16:301.
5. Ma G, Dai W, Sang A, Yang X, Gao C. *Int J Clin Exp Pathol.* 2014;7:8833.
6. Mi S, Lu J, Sun M, et al. *PNAS.* 2007;104:19971.
7. Cheng L, Yang T, Kuang Y, et al. *Oncol Lett.* 2014;7:839.
8. Gottardo F, Liu CG, Ferracin M, et al. *Urologic Oncol.* 2007;25:387.
9. Ciafre SA, Galardi S, Mangiola A, et al. *Biochem Biophys Res Commun.* 2005;334:1351.
10. Huang S, He X, Ding J, et al. *Int J Cancer.* 2008;123:972.
11. Hoy SM. *Drugs.* 2016;76:509.
12. Zhang X, Wu J, Liu W, et al. *Med Chem.* 2017;13:260.
13. Tian H, Liu W, Zhou Z, et al. *Molecules.* 2016;21:1543.
14. Cai W, Wu J, Liu W, et al. *Molecules.* 2018;23:252.
15. Ballatore C, Huryn DM, Smith III AB. *ChemMedChem.* 2013;8:385.
16. Cai W, Liu W, Liu C, Wang J, Zhao G. *Chin J Struct Chem.* 2017;36:897.
17. Miner JN, Tan PK, Hyndman D, et al. *Arthritis Res Ther.* 2016;18:214.
18. Tan PK, Ostertag TM, Miner JN. *Sci Rep.* 2016;6:34995.
19. Miner J, Tan P. *Ann Rheum Dis.* 2013;71:446.
20. Ahn SO, Ohtomo S, Kiyokawa J, et al. *J Pharmacol Exp Ther.* 2016;357:157.
21. Choi Y-J, Larroca V, Lucman A, et al. *Arthritis Rheum.* 2012;64:1632.
22. Mandal A, Emerling D, Serafini T, Mount D. *Arthritis Rheum.* 2010;62:164.
23. Peng J, Hu Q, Gu C, et al. *Bioorg Med Chem Lett.* 2016;26:277.
24. Tian H, Liu Y, Li X, et al. *Chem Res Chin Univ.* 2017;33:587.
25. Brittain JM, de la Mare PB, Newman PA. *J Chem Soc Perkin Trans.* 1981;2:32.
26. Eriksson B., Kurz G., Hedberg C., Westman J. WO2007010273. 2007.
27. Cai W, Liu W, Xie Y, et al. *Chem Res Chin Univ.* 2017;33:49.
28. Brienne MJ, Varech D, Leclercq M, et al. *J Med Chem.* 1987;30:2232.
29. Scholz TH, Sondey JM, Randall WC, et al. *J Med Chem.* 1993;36:2134.
30. Venning AR, Bohan PT, Alexanian EJ. *J Am Chem Soc.* 2015;137:3731.
31. Wojciechowski K, Kosiński S. *Tetrahedron.* 2001;57:5009.
32. Kumar R, Son M, Bavi R, et al. *Acta Pharmacol Sin.* 2015;36:998.
33. Garg D, Gandhi T, Mohan CG. *J Mol Graph Model.* 2008;26:966.
34. Xiao Z, Varma S, Xiao Y-D, Tropsha A. *J Mol Graph Model.* 2004;23:129.
35. Chun S, Lee J-Y, Ro S-G, Jeong K-W, Kim Y-M, Yoon C-J. *Bull Korean Chem Soc.* 2008;29:656.
36. Kristam R, Gillet VJ, Lewis RA, Thorner D. *J Chem Inf Model.* 2005;45:461.
37. Chen W.Y.-C., Chen P.-Y., Chen C.Y.-C., Chung J.-G. Exploring 3D-QSAR pharmacophore mapping of azaphenanthrenone derivatives for mPGES-1 inhibition Using HypoGen technique. Computational Intelligence in Bioinformatics and Computational Biology, 2008. CIBCB'08. IEEE Symposium on. IEEE; 2008:207.
38. Vuorinen A, Engeli R, Meyer A, et al. *J Med Chem.* 2014;57:5995.
39. John S, Thangapandian S, Arooj M, Hong JC, Kim KD, Lee KW Development. evaluation and application of 3D QSAR Pharmacophore model in the discovery of potential human renin inhibitors. *BMC Bioinf 12. BioMed Central.* 2011:S4.
40. Niu M-M, Qin J-Y, Tian C-P, et al. *Acta Pharmacol Sin.* 2014;35:967.
41. Singh A, Singh R. *Open Bioinformatics J.* 2013;7:63.
42. Sakkiah S, Lee KW. *Acta Pharmacol Sin.* 2012;33:964.
43. López-Rodríguez ML, Benhamú B, de la Fuente T, Sanz A, Pardo L, Campillo M. *J Med Chem.* 2005;48:4216.
44. Stoll F, Liesener S, Hohlfeld T, Schrör K, Fuchs PL, Höltje H-D. *Mol Pharmacol.* 2002;62:1103.
45. Zampieri D, Mamolo MG, Laurini E, et al. *J Med Chem.* 2009;52:5380.